Journal of Power Sources 269 (2014) 293–298

Contents lists available at ScienceDirect

Journal of Power Sources

journal homepage: www.elsevier.com/locate/jpowsour

Effect of surface Li_3PO_4 coating on $LiNi_{0.5}Mn_{1.5}O_4$ epitaxial thin film electrodes synthesized by pulsed laser deposition

Hiroaki Konishi [a], Kota Suzuki [a], Sou Taminato [a], Kyungsu Kim [a], Yueming Zheng [a], Sangryun Kim [a], Jaemin Lim [a], Masaaki Hirayama [a], Jin-Young Son [b, c], Yitao Cui [b], Ryoji Kanno [a, *]

[a] Department of Electronic Chemistry, Interdisciplinary Graduate School of Science and Engineering, Tokyo Institute of Technology, 4259 Nagatsuta-cho, Midori-ku, Yokohama 226-8502, Japan
[b] Japan Synchrotron Radiation Research Institute (JASRI), 1-1-1 Kouto, Sayo, Hyogo 679-5198, Japan
[c] SPring-8 Service Co., Ltd., 1-20-5 Kouto, Shingu, Tatsuno, Hyogo 679-5165, Japan

HIGHLIGHTS

- Amorphous Li_3PO_4 was stacked on the epitaxial $LiNi_{0.5}Mn_{1.5}O_4$ films.
- Li_3PO_4 stacking affected the electronic state of the $LiNi_{0.5}Mn_{1.5}O_4$.
- Li_3PO_4 stacking improved the cycling performance of $LiNi_{0.5}Mn_{1.5}O_4$ surface.

ARTICLE INFO

Article history:
Received 2 February 2014
Received in revised form
10 May 2014
Accepted 12 May 2014
Available online 7 July 2014

Keywords:
$LiNi_{0.5}Mn_{1.5}O_4$
Surface coating
Epitaxial thin film
High voltage positive electrode
Spinel
Lithium ion battery

ABSTRACT

The effect of Li_3PO_4 coating was investigated for $LiNi_{0.5}Mn_{1.5}O_4$ epitaxial thin film electrodes synthesized on $SrTiO_3$ substrates by pulsed laser deposition (PLD). Amorphous Li_3PO_4 with a thickness of 1–4 nm was coated at room temperature onto 30 nm thick epitaxial $LiNi_{0.5}Mn_{1.5}O_4$ thin films with (111), (110) and (100) lattice orientations. Electrodes with the surface coating exhibit high charge–discharge capacities and small capacity degradation during cycling experiments in the high voltage region. X-ray absorption near edge structure (XANES) and hard X-ray photoelectron spectroscopy (HAXPES) analyses indicate a higher manganese valence for the electrode surface of the Li_3PO_4 stacked $LiNi_{0.5}Mn_{1.5}O_4$ film than that for the surface of a pristine $LiNi_{0.5}Mn_{1.5}O_4$ film. Thus, surface coating affects the manganese valence near the electrode surface and improves the cycling characteristics.

1. Introduction

Since the discovery of lithium-ion batteries, this extremely useful secondary battery system has been widely applied to small-scale electronic devices such as cellular phones and laptop computers. Further developments in performance have proceeded for application to large-scale devices. Among the current developmental research topics for this battery system, increase in the energy density is an important issue for next-generation batteries, so that high voltage positive electrode materials are very promising.

The transition metal oxide with spinel structure, $LiNi_{0.5}Mn_{1.5}O_4$, is a candidate material for a high-energy battery system due to its high operating voltage [1–3]. The spinel material is stable under cell voltages of 4–5 V, which is much higher than conventional positive electrode materials. Furthermore, this material has the advantages of low cost and low toxicity compared to other conventional electrode materials such as $LiCoO_2$. However, the high operating voltage, which is close to the decomposition potential for conventional electrolytes [4,5], causes rapid capacity degradation, particularly at elevated temperatures [6,7]. To achieve stable and reliable charge–discharge characteristics at high voltage regions, material modification using a surface coating technique is an effective method that has been commonly used to improve battery characteristics. A wide variety of coating materials have been

* Corresponding author. Tel./fax: +81 45 924 5401.
E-mail address: kanno@echem.titech.ac.jp (R. Kanno).

http://dx.doi.org/10.1016/j.jpowsour.2014.05.052
0378-7753/

reported for $LiNi_{0.5}Mn_{1.5}O_4$ to date, such as $AlPO_4$ [8], SiO_2 [9], ZnO [10,11], BiOF [12], ZrP_2O_7 [13], ZrO_2 [13], and such coating was found to be very efficient for improvement of the charge and discharge characteristics. Although mechanistic studies using impedance spectroscopy and transmission electron microscopy (TEM) analysis have emphasized the importance of interfacial reactions [6–15], a detailed reaction mechanism has yet to be clarified.

Recently, epitaxial thin films have been proposed as an ideal model system for mechanistic studies to clarify the electrochemical reactions that occur at the electrode surface because of the following advantages [16–18]: (i) epitaxial thin films provide a flat electrode surface with a roughness of less than 1 nm, (ii) anisotropic reactions dependent on the crystal lattice orientation can be detected because the orientation of thin film is controlled by the choice of substrate orientation, (iii) thin films with nanosized (<100 nm) electrodes can be easily fabricated by changing the film deposition period, and (iv) the influence of the conducting material and binder for the reaction mechanism can be eliminated.

Epitaxial thin films of $LiNi_{0.5}Mn_{1.5}O_4$ were synthesized on $SrTiO_3$ substrates with the lattice orientation controlled by changing the substrate orientation; $LiNi_{0.5}Mn_{1.5}O_4$ films with (111), (110) and (100) orientations were synthesized and their electrochemical characteristics were clarified. Although the $LiNi_{0.5}Mn_{1.5}O_4$ films have high discharge capacities, they showed poor cycling performance [19]. Further studies to improve the cycling characteristics at high voltages and mechanistic studies in the high voltage region have been required.

In the present study, the effect of Li_3PO_4 coating for $LiNi_{0.5}Mn_{1.5}O_4$ has been studied using epitaxial thin film model electrodes. The Li_3PO_4 solid-electrolyte was coated onto $LiNi_{0.5}Mn_{1.5}O_4$ thin films synthesized on the $SrTiO_3$ substrates with (111), (110) and (100) orientations by pulsed laser deposition (PLD) in an attempt to improve the electrochemical characteristics. The reaction mechanism of Li_3PO_4 coated $LiNi_{0.5}Mn_{1.5}O_4$ films was examined using X-ray diffraction (XRD), X-ray absorption near edge structure (XANES), and hard X-ray photoelectron spectroscopy (HAXPES) measurements.

2. Experimental

$LiNi_{0.5}Mn_{1.5}O_4$ and Li_3PO_4 coated $LiNi_{0.5}Mn_{1.5}O_4$ thin films were grown on single-crystal $SrTiO_3$(111), (110) and (100) substrates. A $SrRuO_3$ layer was fabricated between the $LiNi_{0.5}Mn_{1.5}O_4$ film and the substrate as a buffer layer to provide high electronic conductivity at the substrate–electrode interface and improve the charge-and-discharge characteristics [20]. The films were synthesized using a KrF excimer laser with a wavelength of 248 nm and a PLD system (PLAD312, AOV. Inc.). The substrates were washed with ultrapure water and annealed at 1000 °C under oxygen gas flow. After the annealing treatment, gold was deposited on both the back and lateral sides of the substrates using a sputtering system (Quick Coater SC-701, Sanyu Electron Co., Ltd.). The $LiNi_{0.5}Mn_{1.5}O_4$ target was fabricated by the solid-state reaction of Li_2CO_3, NiO and MnO_2 as starting materials. The starting materials were thoroughly mixed, pelletized, and calcined at 1000 °C for 12 h, followed by subsequent heating at 700 °C for 24 h under an oxygen atmosphere. The $LiNi_{0.5}Mn_{1.5}O_4$ target had an excess lithium content [Li/(Ni + Mn) = 0.6] to compensate for lithium loss during the PLD process. Sintered $SrRuO_3$ (Toshima Manufacturing Co., Ltd.) was used as the PLD target. The Li_3PO_4 target was synthesized by calcining γ-Li_3PO_4 at 850 °C for 12 h in air. Table 1 summarizes the PLD conditions employed for each thin film. After deposition of the $SrRuO_3$ layer, the substrates were cooled to room temperature and then reheated to 650 °C for $LiNi_{0.5}Mn_{1.5}O_4$ deposition. The substrates were then cooled to room temperature and Li_3PO_4 was deposited on the surface of the electrodes. The entire process for the deposition of multiple layers was performed in a vacuum chamber to avoid surface contamination during the synthesis procedure.

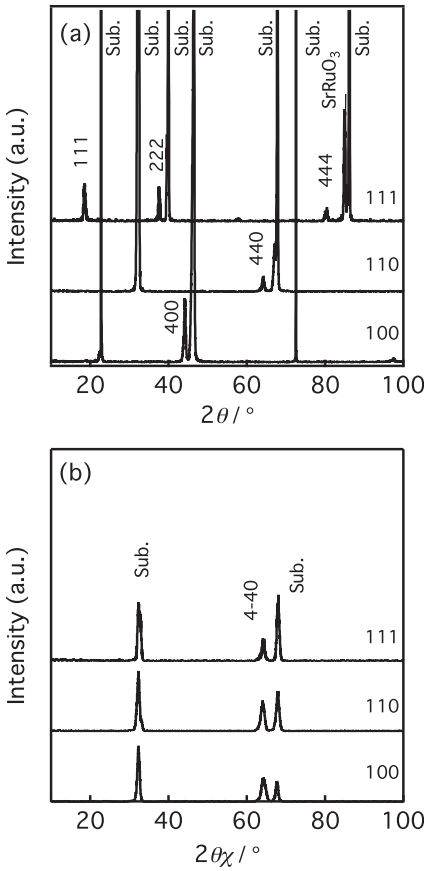

Fig. 1. XRD patterns for $Li_3PO_4/LiNi_{0.5}Mn_{1.5}O_4$ thin films deposited on $SrTiO_3$(111), (110) and (100) substrates: (a) out-of-plane and (b) in-plane patterns along the [1-10]($SrTiO_3$ (111), (110)) and [011] ($SrTiO_3$ (100)) direction of the substrates.

Thin film X-ray diffraction (XRD) patterns were recorded using a diffractometer (ATX-G, Rigaku) with Cu $K\alpha_1$ radiation. The thin film orientations were characterized using out-of-plane and in-plane measurements. The thickness, density, and surface roughness were determined by X-ray reflectivity (XRR) analysis using Parratt32 software [21].

Table 1
PLD conditions for Li_3PO_4, $LiNi_{0.5}Mn_{1.5}O_4$ and $SrRuO_3$ thin films deposited on the $SrTiO_3$(111), (110) and (100) substrates.

Target	Frequency *f*/Hz	Time *t*/min	Pressure *P*/Pa	Temperature *T*/°C	Distance *d*/mm	Energy *E*/mJ
Li_3PO_4	10	3	3.3	25	60	150
$LiNi_{0.5}Mn_{1.5}O_4$	10	60	6.6	650	60	150
$SrRuO_3$	5	30	10	700	60	200

Table 2
Lattice parameters calculated from out-of-plane and in-plane XRD measurements for $LiNi_{0.5}Mn_{1.5}O_4$ and $Li_3PO_4/LiNi_{0.5}Mn_{1.5}O_4$ thin films deposited on the $SrTiO_3$(111), (110) and (100) substrates.

$LiNi_{0.5}Mn_{1.5}O_4$ orientation	Coating	Out-of-plane lattice parameter a/Å	In-plane lattice parameter a/Å
111	Non-coated (Ref. [19])	8.23	8.29
	Li_3PO_4	8.17	8.20
110	Non-coated (Ref. [19])	8.27	8.29
	Li_3PO_4	8.19	8.22
100	Non-coated (Ref. [19])	8.28	8.24
	Li_3PO_4	8.20	8.19

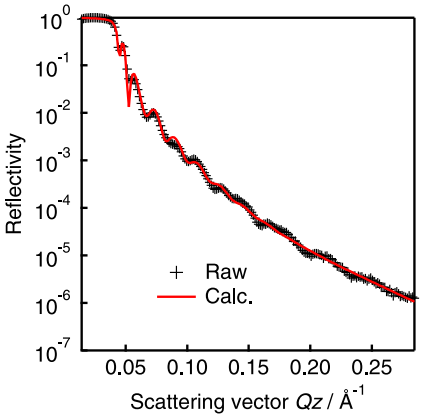

Fig. 2. XRR spectrum and fitting curve for $Li_3PO_4/LiNi_{0.5}Mn_{1.5}O_4$ thin film deposited on the $SrTiO_3$(111) substrate.

Charge–discharge measurements were examined using 2032-type coin cells assembled in an argon-filled glove box with lithium metal as the counter electrode and the $LiNi_{0.5}Mn_{1.5}O_4$ thin film as the working electrode. The electrolyte employed was ethylene carbonate (EC)/diethyl carbonate (DEC) in a molar ratio of 3:7 as a solvent with a supporting electrolyte of 1 M $LiPF_6$. The charge–discharge characteristics of the epitaxial films were examined in the range of 3.2–5.0 V with a current density of 1.1 μA cm^{-2} (TOSCAT–3100, Toyo System Co., Ltd). The capacities of the thin films were calculated from the deposited area (10 × 9 mm^2).

Mn K-edge XANES measurements were performed in fluorescence mode using a germanium single-element solid-state detector (Ge SSD) installed at the BL14B2 beamline of SPring-8, Japan.

HAXPES measurements were performed to evaluate the electric structures of the thin film electrodes after the cell was galvanostatically cycled between 3.2 and 5.0 V. HAXPES measurements were performed using a hemispherical electronanalyzer (VG-SIENTA R-4000) installed at the in-vacuum undulator BL46XU beamline of

Table 3
XRR analysis results for $Li_3PO_4/LiNi_{0.5}Mn_{1.5}O_4$ thin films deposited on the $SrTiO_3$(111), (110) and (100) substrates.

Substrate orientation	Layer	Thickness t/nm	Density d/g cm^{-3}	Roughness r/nm
$SrTiO_3$(111)	Li_3PO_4	1.1	2.0	0.5
	$LiNi_{0.5}Mn_{1.5}O_4$	30.6	4.5	1.3
	$SrRuO_3$	15.1	6.3	1.8
$SrTiO_3$(110)	Li_3PO_4	3.6	1.8	0.7
	$LiNi_{0.5}Mn_{1.5}O_4$	29.0	4.5	2.8
	$SrRuO_3$	20.4	6.2	3.5
$SrTiO_3$(100)	Li_3PO_4	0.7	2.1	0.2
	$LiNi_{0.5}Mn_{1.5}O_4$	26.5	4.5	0.9
	$SrRuO_3$	13.6	6.0	1.4

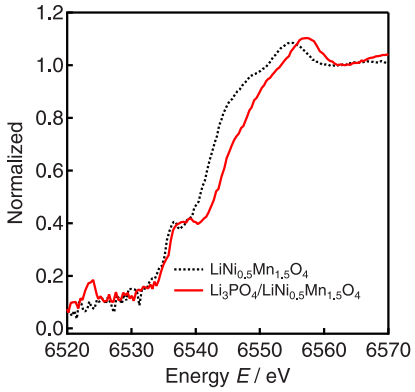

Fig. 3. Mn K-edge XANES spectra for $LiNi_{0.5}Mn_{1.5}O_4$(111) and $Li_3PO_4/LiNi_{0.5}Mn_{1.5}O_4$(111) thin films.

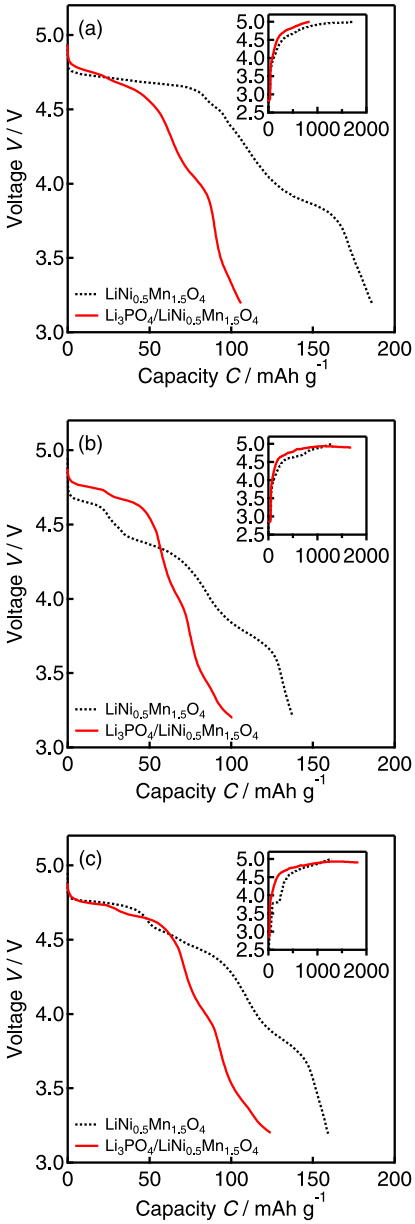

Fig. 4. Charge–discharge curves of the 1st cycle for (a) $LiNi_{0.5}Mn_{1.5}O_4$(111), $Li_3PO_4/LiNi_{0.5}Mn_{1.5}O_4$(111), (b) $LiNi_{0.5}Mn_{1.5}O_4$(110), $Li_3PO_4/LiNi_{0.5}Mn_{1.5}O_4$(110) and (c) $LiNi_{0.5}Mn_{1.5}O_4$(100), $Li_3PO_4/LiNi_{0.5}Mn_{1.5}O_4$(100) thin films.

SPring-8, Japan. The X-rays were monochromated using a Si(111) double crystal system. The binding energy was calibrated using the Au $4f_{7/2}$ peak at 84.0 eV of a gold reference sample. The X-ray energy of 7940 eV was selected to enhance the probe depth. The probe depth can be controlled by regulating the photoelectron take-off-angle (TOA) of 80°, which corresponds to the electronic structure of the $LiNi_{0.5}Mn_{1.5}O_4$ thin film inside the coating layer.

3. Results and discussion

3.1. Structure of Li_3PO_4 stacked $LiNi_{0.5}Mn_{1.5}O_4$ thin film

XRD and XRR analyses were applied to characterize the Li_3PO_4 coated $LiNi_{0.5}Mn_{1.5}O_4$ thin films ($Li_3PO_4/LiNi_{0.5}Mn_{1.5}O_4$) deposited on $SrTiO_3$(111), (110) and (100) substrates. Fig. 1 shows out-of-plane and in-plane XRD patterns for $Li_3PO_4/LiNi_{0.5}Mn_{1.5}O_4$ thin films deposited on $SrTiO_3$(111), (110) and (100) substrates. The diffraction patterns show reflections due to $LiNi_{0.5}Mn_{1.5}O_4$, while no reflection peaks from the coated Li_3PO_4 film were observed. These results indicate that the Li_3PO_4 coating does not affect the orientation of the $LiNi_{0.5}Mn_{1.5}O_4$ thin films and that the Li_3PO_4 film is amorphous. The $LiNi_{0.5}Mn_{1.5}O_4$ thin films have lattice orientations of (111), (110) and (100) that correspond to the $SrTiO_3$(111), (110) and (100) substrates, respectively [19]. Table 2 summarizes the calculated lattice parameters determined from the out-of-plane and in-plane XRD measurements. The lattice parameters of the $LiNi_{0.5}Mn_{1.5}O_4$(111), (110) and (100) thin films calculated from out-of-plane measurements decreased from 8.23, 8.27, and 8.28 to 8.17, 8.19, and 8.20 Å, respectively, with the Li_3PO_4 coating. The lattice parameters of the thin films calculated from in-plane measurements showed the same tendency. The Li_3PO_4 coating affects the structure of the films and results in a lattice that is smaller than the pristine film. Fig. 2 shows XRR spectrum and fitting curve for the $Li_3PO_4/LiNi_{0.5}Mn_{1.5}O_4$ thin film deposited on a $SrTiO_3$(111) substrate. The spectrum is plotted as a function of the scattering vector, $Qz = 4\pi\sin\theta/\lambda$, where λ is the X-ray wavelength (1.541 Å) and θ is the incident angle. A three-layer model consisting of the Li_3PO_4 layer, $LiNi_{0.5}Mn_{1.5}O_4$ layer and the buffer $SrRuO_3$ layer was applied for the fittings. Table 3 summarizes the fitting results for the XRR analysis and those reported for the pristine samples. The thickness and density of $LiNi_{0.5}Mn_{1.5}O_4$ and $SrRuO_3$ in the $Li_3PO_4/LiNi_{0.5}Mn_{1.5}O_4$ thin films are almost the same as those observed for the $LiNi_{0.5}Mn_{1.5}O_4$ films reported previously [19]. The thicknesses and densities of the stacked Li_3PO_4 films were 0.7–3.6 nm and 1.8–2.1 g cm^{-3}, respectively, for all film orientations. The observed densities of 1.8–2.1 g cm^{-3} are slightly lower than that of the bulk crystalline material, γ-Li_3PO_4 (d = 2.43 g cm^{-3}).

Fig. 3 shows Mn K-edge XANES spectra for the $LiNi_{0.5}Mn_{1.5}O_4$(111) and $Li_3PO_4/LiNi_{0.5}Mn_{1.5}O_4$(111) thin films. The half-height energy ($\mu t = 0.5$) shifts to higher energy with the Li_3PO_4 coating, which indicates an increase in the manganese valence [22]. Thus, the Li_3PO_4 coating affects the manganese valence state of the $LiNi_{0.5}Mn_{1.5}O_4$ surface. The change in the valence state of manganese ions could be explained by the following. (i) The positive electrode surface is in direct contact with moisture and carbon dioxide in the open atmosphere, so that the manganese valence state at the surface may be changeable [23,24]. Surface coating may suppress the direct contact between the $LiNi_{0.5}Mn_{1.5}O_4$ surface and

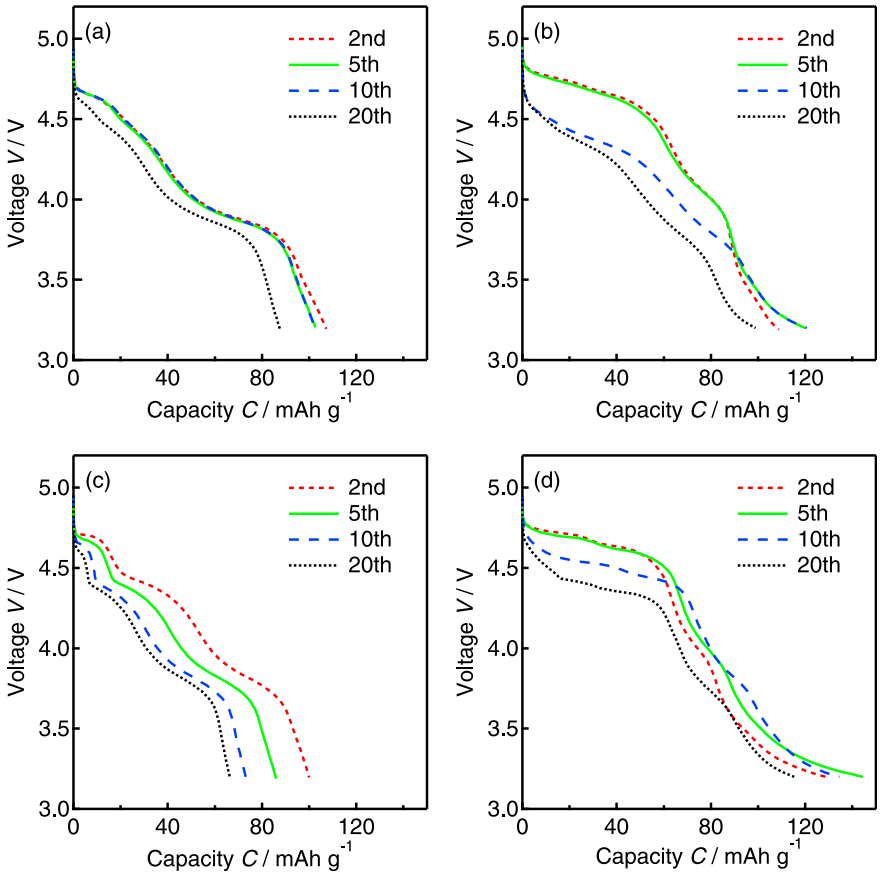

Fig. 5. Discharge curves of the 2nd, 5th, 10th and 20th cycles for (a) $LiNi_{0.5}Mn_{1.5}O_4$(111), (b) $Li_3PO_4/LiNi_{0.5}Mn_{1.5}O_4$(111), (c) $LiNi_{0.5}Mn_{1.5}O_4$(100) and (d) $Li_3PO_4/LiNi_{0.5}Mn_{1.5}O_4$(100) thin films.

the atmosphere. (ii) The Li_3PO_4 coating layer may act as an electrolyte when in contact with the $LiNi_{0.5}Mn_{1.5}O_4$ surface, and this may therefore change the electronic state of $LiNi_{0.5}Mn_{1.5}O_4$ with the formation of an electronic double (space charge) layer in the interfacial region. A space charge layer is formed between two different phases with different chemical potentials and lithium-ion diffusion at the interfacial boundary region can be affected by the change in the electronic state [25–27]. Further studies on the electronic structure at the interfacial region are necessary to confirm such physical phenomena at the boundary.

3.2. Electrochemical properties of $Li_3PO_4/LiNi_{0.5}Mn_{1.5}O_4$ thin films

Fig. 4 shows charge–discharge curves of the 1st cycle for $Li_3PO_4/LiNi_{0.5}Mn_{1.5}O_4$ thin films with (111), (110) and (100) orientations, together with those of $LiNi_{0.5}Mn_{1.5}O_4$ reported previously [19].

The charge capacities of these films exceed their theoretical capacities (148 mAh g^{-1}) because the reaction voltage of $LiNi_{0.5}Mn_{1.5}O_4$ is close to the decomposition voltage of EC/DEC (5.0 V) [5]. The Li_3PO_4 coating on the surface affects the discharge behavior of $LiNi_{0.5}Mn_{1.5}O_4$ with all orientations, which might be related to the crystal structure of $LiNi_{0.5}Mn_{1.5}O_4$. The $LiNi_{0.5}Mn_{1.5}O_4$ spinel has been reported to have two types of crystal structures; an ordered $LiNi_{0.5}Mn_{1.5}O_4$ spinel structure with the space group $P4_332$ and a disordered spinel structure with a composition of $LiNi_{0.5}Mn_{1.5}O_{4-\delta}$ and the space group Fd-3m. The charge–discharge reaction of the ordered $LiNi_{0.5}Mn_{1.5}O_4$ proceeds via the Ni^{2+}/Ni^{4+} redox couple with only one voltage plateau around 4.7 V. In contrast, the oxygen deficient disordered $LiNi_{0.5}Mn_{1.5}O_{4-\delta}$ contains trivalent manganese and exhibits two voltage plateaus in the charge–discharge curves at around 4.7 V (Ni^{2+}/Ni^{4+}) and 4.1 V (Mn^{3+}/Mn^{4+}) [28–32].

Fig. 4(a) shows charge–discharge curves of the 1st cycle for the $LiNi_{0.5}Mn_{1.5}O_4$(111) and Li_3PO_4 coated $LiNi_{0.5}Mn_{1.5}O_4$(111) thin films. Two plateaus at around 4.7 and 3.9 V are observed in both films. However, the Mn^{3+}/Mn^{4+} plateau for the coated $LiNi_{0.5}Mn_{1.5}O_4$ film is smaller than that of the non-coated $LiNi_{0.5}Mn_{1.5}O_4$ film, which indicates that the Mn^{3+}/Mn^{4+} ratio is decreased with Li_3PO_4 coating. This is consistent with the XANES measurement results, which indicate higher manganese valence for the Li_3PO_4 coated samples.

Fig. 4(b) and (c) shows charge–discharge curves of the 1st cycle for the $LiNi_{0.5}Mn_{1.5}O_4$ and $Li_3PO_4/LiNi_{0.5}Mn_{1.5}O_4$ films with (110) and (100) orientations. The Mn^{3+}/Mn^{4+} redox reaction was suppressed by the Li_3PO_4 coating, similarly to that observed for the $Li_3PO_4/LiNi_{0.5}Mn_{1.5}O_4$(111) film, and no significant differences in the discharge curves and electrochemical characteristics were observed for these different orientations of the coated films.

Fig. 5 shows the discharge curves of the 2nd, 5th, 10th and 20th cycles of the $LiNi_{0.5}Mn_{1.5}O_4$ and $Li_3PO_4/LiNi_{0.5}Mn_{1.5}O_4$ films with the (111) and (100) orientations. The discharge capacities of $Li_3PO_4/LiNi_{0.5}Mn_{1.5}O_4$(111) film were larger than those of the $LiNi_{0.5}Mn_{1.5}O_4$(111) film. The Li_3PO_4 coating improved the cycling performance for the $LiNi_{0.5}Mn_{1.5}O_4$(100) film, as shown in Fig. 5(c) and (d). Although the capacity degradation of the coated films was rather small, a decrease in the cell voltage around 4.7 V was observed in the 10th and 20th cycles. This may correspond to an increase in the cell resistance, which might be due to an increase in the solid electrolyte interphase (SEI) layer formed by oxidation of the electrolyte [5,33].

3.3. The oxidation state after the 1st cycle

Fig. 6 shows $Mn2p_{3/2}$ HAXPES spectra and their fitting curves for $LiNi_{0.5}Mn_{1.5}O_4$(111) and $Li_3PO_4/LiNi_{0.5}Mn_{1.5}O_4$(111) thin films after the 1st charge–discharge cycle. The spectra were collected at a TOA of 80°, which corresponds to the electronic structure of the thin films inside the coating layer. The $Mn2p_{3/2}$ spectra of both films can be divided into two peaks around 641.9 and 642.8 eV, which are attributed to the Mn^{3+} and Mn^{4+} states, respectively [34,35]. The peak intensity for Mn^{3+} in $Li_3PO_4/LiNi_{0.5}Mn_{1.5}O_4$(111) film is smaller than that of the $LiNi_{0.5}Mn_{1.5}O_4$(111) film, which indicates a higher manganese valence in the coated film. The trivalent manganese valence, Mn^{3+}, is present in both the initial state and after the 1st charge–discharge cycle for the surface of $LiNi_{0.5}Mn_{1.5}O_4$ without the Li_3PO_4 coating. A lower manganese valence state causes manganese dissolution [36,37] and lattice distortion by the Jahn–Teller effect [38,39], which may also be related to the degradation in capacity. The Li_3PO_4 coating changes the manganese valence state of the electrode surface and maintains a slightly higher manganese valence state, which may improve the charge–discharge characteristics. The change in the manganese valence state may also be attributed to a difference in the chemical potential between Li_3PO_4 and $LiNi_{0.5}Mn_{1.5}O_4$ and the resultant formation of a space charge layer [25–27]. Further studies on the structure and electronic state are necessary to confirm the formation of the deficient phases at the two-phase boundary region.

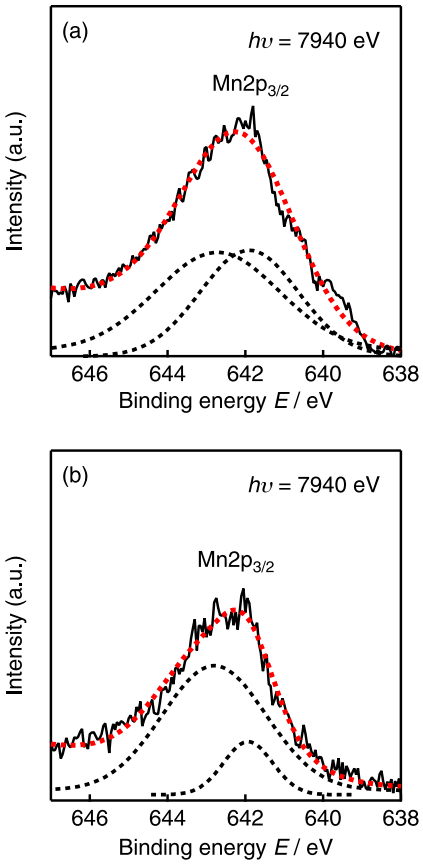

Fig. 6. $Mn2p_{3/2}$ HAXPES spectra and fitting curves after 1st cycle for (a) $LiNi_{0.5}Mn_{1.5}O_4$(111) and (b) $Li_3PO_4/LiNi_{0.5}Mn_{1.5}O_4$(111) thin films.

4. Conclusions

The effects of surface coating on high voltage positive electrode materials with the spinel structure were examined. Amorphous Li_3PO_4 was coated onto epitaxial $LiNi_{0.5}Mn_{1.5}O_4$ thin film at room temperature without changing the orientation of $LiNi_{0.5}Mn_{1.5}O_4$

films. However, the coating affected the lattice parameter, electronic state of manganese and electrochemical properties. The improved cycling performance was explained by the change in the manganese valence state at the surface of the electrode. A higher valence state at the surface region by Li_3PO_4 coating reduces the manganese dissolution and lattice distortion of the electrode, which improves the cycling characteristics. These results indicate that controlling the electronic state of manganese at the surface is important to improve the stability of $LiNi_{0.5}Mn_{1.5}O_4$ surface.

Acknowledgment

The synchrotron radiation experiments were performed as projects approved by the Japan Synchrotron Radiation Research Institute (JASRI) (Proposal Nos. 2012B1679 and 2012B1741). This study was partly supported by a Grant-in-Aid for Scientific Research on Innovative Areas “Exploration of nano-structure–property relationships for materials innovation” from the Japan Society for the Promotion of Science (No. 25106009).

References

[1] Q. Zhong, A. Bonakdarpour, M. Zhang, Y. Gao, J.R. Dahn, J. Electrochem. Soc. 144 (1997) 205–213.
[2] T. Ohzuku, K. Ariyoshi, S. Yamamoto, Y. Makimura, Chem. Lett. (2001) 1270–1271.
[3] K. Ariyoshi, Y. Iwakoshi, N. Nakayama, T. Ohzuku, J. Electrochem. Soc. 151 (2004) A296–A303.
[4] L. Yang, B. Ravdel, B.L. Lucht, Electrochem. Solid-State Lett. 13 (2010) A95–A97.
[5] W. Xu, X. Chen, F. Ding, J. Xiao, D. Wang, A. Pan, J. Zheng, X.S. Li, A.B. Padmaperuma, J.G. Zhang, J. Power Sources 213 (2012) 304–316.
[6] T. Yoon, S. Park, J. Mun, J.H. Ryu, W. Choi, Y.S. Kang, J.H. Park, S.M. Oh, J. Power Sources 215 (2012) 312–316.
[7] J. Mao, K. Dai, Y. Zhai, Electrochim. Acta 63 (2012) 381–390.
[8] J.Y. Shi, C.W. Yi, K. Kim, J. Power Sources 195 (2010) 6860–6866.
[9] Y. Fan, J. Wang, Z. Tang, W. He, J. Zhang, Electrochim. Acta 52 (2007) 3870–3875.
[10] Y.K. Sun, C.S. Yoon, I.H. Oh, Electrochim. Acta 48 (2003) 503–506.
[11] J.C. Arrebola, A. Caballero, L. Hernan, J. Morales, J. Power Sources 195 (2010) 4278–4284.
[12] H.B. Kang, S.T. Myung, K. Amine, S.M. Lee, Y.K. Sun, J. Power Sources 195 (2010) 2023–2028.
[13] H.M. Wu, I. Belharouak, A. Abouimrane, Y.K. Sun, K. Amine, J. Power Sources 195 (2010) 2909–2913.
[14] T. Yang, N. Zhang, Y. Lang, K. Sun, Electrochim. Acta 56 (2011) 4058–4064.
[15] Y.Y. Huang, X.L. Zeng, C. Zhou, P. Wu, D.G. Tong, J. Mater. Sci. 48 (2013) 625–635.
[16] M. Hirayama, N. Sonoyama, M. Ito, M. Minoura, D. Mori, A. Yamada, K. Tamura, J. Mizuki, R. Kanno, J. Electrochem. Soc. 154 (2007) A1065–A1072.
[17] K. Sakamoto, H. Konishi, N. Sonoyama, A. Yamada, K. Tamura, J. Mizuki, R. Kanno, J. Power Sources 174 (2007) 678–682.
[18] M. Hirayama, H. Ido, K. Kim, W. Cho, K. Tamura, J. Mizuki, R. Kanno, J. Am. Chem. Soc. 132 (2010) 15268–15276.
[19] H. Konishi, K. Suzuki, S. Taminato, K. Kim, S. Kim, J. Lim, M. Hirayama, R. Kanno, J. Power Sources 246 (2014) 365–370.
[20] K. Suzuki, K. Kim, S. Taminato, M. Hirayama, R. Kanno, J. Power Sources 226 (2013) 340–345.
[21] L.G. Parratt, Phys. Rev. 95 (1954) 359–369.
[22] D. Pasero, N. Reeves, V. Pralong, A.R. West, J. Electrochem. Soc. 155 (2008) A282–A291.
[23] R. Moshtev, P. Zlatilova, S. Vasilev, I. Bakalova, A. Kozawa, J. Power Sources 81–82 (1999) 434–441.
[24] K. Matsumoto, R. Kuzuo, K. Takeya, A. Yamanaka, J. Power Sources 81–82 (1999) 558–561.
[25] N. Ohta, K. Takada, L. Zhang, R. Ma, M. Osada, T. Sasaki, Adv. Mater. 28 (2006) 2226–2229.
[26] N. Ohta, K. Takada, I. Sakaguchi, L. Zhang, R. Ma, K. Fukuda, M. Osada, T. Sasaki, Electrochem. Commun. 9 (2007) 1486–1490.
[27] H. Yamada, Y. Oga, I. Saruwatari, I. Moriguchi, J. Electrochem. Soc. 159 (2012) A380–A385.
[28] Y. Idemoto, H. Narai, N. Koura, J. Power Sources 119–121 (2003) 125–129.
[29] J.H. Kim, S.T. Myung, C.S. Yoon, S.G. Kang, Y.K. Sun, Chem. Mater. 16 (2004) 906–914.
[30] M. Kunduraci, J.F. Al-Sharab, G.G. Amatucci, Chem. Mater. 18 (2006) 3585–3592.
[31] X. Fang, N. Ding, X.Y. Feng, Y. Lu, C.H. Chen, Electrochim. Acta 54 (2009) 7471–7475.
[32] Y.C. Jin, C.Y. Lin, J.G. Duh, Electrochim. Acta 69 (2012) 45–50.
[33] M. Matsui, K. Dokko, K. Kanamura, J. Electrochem. Soc. 157 (2010) A121–A129.
[34] T.F. Yi, X.G. Hu, J. Power Sources 167 (2007) 185–191.
[35] Y. Wei, K.B. Kim, G. Chen, Electrochim. Acta 51 (2006) 3365–3373.
[36] J.C. Hunter, J. Solid State Chem. 39 (1981) 142–147.
[37] Y. Liu, X. Li, H. Guo, Z. Wang, Q. Hu, W. Peng, Y. Yang, J. Power Sources 189 (2009) 721–725.
[38] R.J. Gummow, A. deKock, M.M. Thackeray, Solid State Ionics 69 (1994) 59–67.
[39] E. Wolska, M. Tovar, B. Andrzejewski, W. Nowicki, J. Darul, P. Piszora, M. Knapp, Solid State Sci. 8 (2006) 31–36.